In Situ STM Investigation of Gold Reconstruction and of Silicon Electrodeposition on Au(111) in the Room Temperature Ionic Liquid 1-Butyl-1-methylpyrrolidinium Bis(trifluoromethylsulfonyl)imide

N. Borisenko, S. Zein El Abedin,† and F. Endres*

Faculty of Natural and Materials Sciences, Clausthal University of Technology, Robert-Koch-Strasse 42, D-38678 Clausthal-Zellerfeld, Germany

Received: December 15, 2005; In Final Form: February 7, 2006

The electrodeposition of silicon on Au(111) was investigated by cyclic voltammety (CV) and by in situ scanning tunneling microscopy (STM) in the room temperature ionic liquid 1-butyl-1-methylpyrrolidinium bis(trifluoromethylsulfonyl)imide with a $SiCl_4$ concentration of 0.1 mol/L. A main reduction process begins in the cyclic voltammogram at about −1800 mV versus ferrocene/ferrocinium, which is correlated to the electrodeposition of elemental semiconducting silicon. It has been found that at an electrode potential more negative than the open circuit potential (OCP), the Au(111) surface is subject to a restructuring/reconstruction both in the case of the pure ionic liquid and in the presence of $SiCl_4$. The first STM-probed silicon islands with 150−450 pm in height appear at about −1700 mV versus ferrocene/ferrocinium. Their lateral and vertical growth leads to the formation of a rough layer with silicon islands of up to 1 nm in height. At about −1800 mV the islands merge and form silicon agglomerates. In situ I/U tunneling spectroscopy reveals a band gap of 1.1 ± 0.2 eV for layers of about 5 nm in height, a value that has to be expected for semiconducting silicon.

Introduction

Since its invention, scanning tunneling microscopy (STM) has been extensively used for investigations of surfaces and interfaces under different conditions. There are numerous studies on nanoscale electrochemical phase formation on a variety of substrates in aqueous solutions, organic solvents, and, recently, ionic liquids.[1−14] The investigation of phase formation processes during semiconductor electrodeposition has been of a great interest in recent studies.[15−17] A controlled electrodeposition of nanocrystalline semiconductors would also be interesting for nanotechnology.[18] Semiconductor nanoparticles with the diameter of 1−20 nm are especially interesting because they exhibit a change in their electronic properties relative to the bulk material. When the size of the particles decreases, the band gap increases. It is known that silicon nanoclusters can luminesce in the red region of the visible spectrum. When an electric current is passed or ultraviolet light is illuminated, the nanometer-sized silicon particles can also luminesce in the blue region of the visible spectrum. This provides an opportunity to apply them in making displays and indicator lights, as blue luminescence is not often seen in other semiconductor systems existing nowadays.

Silicon nanocrystals embedded in a SiO_2 matrix can be used for nanoscale silicon-based laser development.[19] There are various methods for the synthesis of nanoscale silicon:[20] gas-phase decomposition of silanes, ultrasonic dispersion of porous silicon in different solvents, and electrochemical synthesis. In the first method, a series of higher silanes, disilanes, and silylene polymeric species is formed at high temperatures (850−1050 °C) in an enclosed vessel. In the second method, a colloid with particles of 1−10 nm and agglomerates of up to 50 nm in size is formed. However, both methods are quite expensive, and it is difficult to control the size distribution of nanoparticles.

Electrochemistry, on the other hand, is a valuable tool as by variation of the parameters (such as electrode potential, current density, and concentration of the electrolyte) the structure and the size of the deposit can be adjusted. However, the electrochemical phase formation in aqueous solutions is restricted: at the cathodic limit hydrogen is formed, and at the anodic limit either oxygen forms or the electrode material is oxidized, resulting in an electrochemical window of only about 1.2 V. Therefore, elemental semiconductors such as silicon, germanium, and their mixtures (Si_xGe_{1-x}) cannot be obtained from aqueous solutions. There were several attempts in the past to electrodeposit silicon from organic solvents,[21−23] and smooth and uniform silicon deposits up to 0.25 μm thick could be obtained. However, Auger electron spectroscopy analysis of such a deposit gave oxygen content, and it was not clear whether the deposit was oxidized during the deposition process or if it was a consequence of an open porosity in the film.

In the case of germanium electrodeposition, GeI_4 dissolved in propylene glycol has been proposed as a suitable system,[24] but macroscopically thick and amorphous germanium films were obtained only at temperatures of ≥100 °C under galvanostatic conditions with current densities up to 0.2 A cm^{-2}. Szekeley reported that a roughly 130 μm thick germanium layer was electrodeposited from $GeCl_4$ dissolved in propylene glycol at 59 °C and a constant current density of 0.4 mA cm^{-2}.[25] However, the current efficiency of this system was only about 1%. Furthermore, silicon can be obtained in high-temperature molten salts.[26] Katayama et al.[27] reported that a thin silicon layer can be electrodeposited from 1-ethyl-3-methylimidazolium

* Corresponding author (telephone +49-5323-72-3141; fax +49-5323-72-2460; e-mail frank.endres@tu-clausthal.de).
† Permanent address: Electrochemistry and Corrosion Laboratory, National Research Centre, Dokki, Cairo, Egypt.

10.1021/jp057337d CCC: $33.50
Published on Web 03/03/2006

hexafluorosilicate at 90 °C. Upon exposure to air the deposit reacted completely to SiO_2. Thus, it is an open question whether the obtained silicon was semiconducting. The electrodeposition of silicon from its halides in nonaqueous solutions has been described quite recently.[28] As can be expected, the authors also report a strong oxidation of the electrochemically made silicon. In previous studies we have shown that, due to their extraordinarily wide electrochemical windows (up to 6 V), low vapor pressure, and high chemical stability, ionic liquids can be used for the electrodeposition of semiconductors. It was shown that elemental germanium can be electrodeposited from germanium halides dissolved in the room temperature ionic liquid 1-butyl-3-methylimidazolium hexafluorophosphate. With the help of in situ STM and in situ current/voltage tunneling spectroscopy, it was shown that germanium layers with a thickness of ≥ 20 nm are semiconducting with a symmetric band gap of 0.7 ± 0.1 eV.[29−31] In the case of silicon we have shown for the first time that semiconducting silicon can be electrodeposited in the room temperature ionic liquid 1-butyl-1-methylpyrrolidinium bis-(trifluoromethylsulfonyl)imide ([BMP]Tf_2N) saturated with $SiCl_4$. The investigations were performed on highly oriented pyrolytic graphite (HOPG), and a silicon layer with a thickness of 100 nm exhibiting a band gap of 1.0 ± 0.2 eV was obtained.[32] A disadvantage of HOPG as a substrate is that there is a weak interaction between substrate and deposit, thus making STM investigations difficult. Well-defined Au(111) is a much better substrate for such purposes. It is well-known that Au(111) is subject to restructuring/reconstruction, especially under electrochemical control in aqueous solutions (see ref 33 and references cited therein). In ionic liquids there is only one paper available in the literature,[34] but the authors employed an extremely difficult to purify and water-containing hexafluorophosphate ionic liquid. Thus, it is questionable if the restructuring/reconstruction is really an effect of the ionic liquid or of byproducts and water.

Reliable information on restructuring/reconstruction of metal surfaces in ionic liquids is currently completely missing. In the present paper we show for the first time a detailed in situ STM study of the electrochemical behavior of Au(111) in the pure ionic liquid [BMP]Tf_2N and of the silicon electrodeposition from $SiCl_4$ (0.1 M) in this ionic liquid on Au(111). We show that Au(111) is subject to a potential dependent restructuring/reconstruction both in the pure ionic liquid and in the presence of $SiCl_4$. We find that a thin, only about 5 nm thick, silicon layer is semiconducting with a symmetrical band gap of 1.1 ± 0.2 eV.

Experimental Section

[BMP]Tf_2N ionic liquid was purchased from Merck/EMD in ultrapure quality (chloride < 10 ppm, Li-free synthesis). This ionic liquid has a wide electrochemical window of about 5 V on Au(111) and an acceptable viscosity of 85 mPa s at 25 °C.[35] Before use, the liquid was dried under vacuum at 120 °C to water contents well below 1 ppm and stored in a closed bottle in an argon-filled glovebox with water and oxygen contents below 2 ppm (OMNI-LAB from Vacuum-Atmospheres). $SiCl_4$ (99.999%) was purchased from Alfa Aesar. The working electrode was Au(111) (gold on mica), purchased from Molecular Imaging. The substrates were annealed at 350 °C for 4 h in a quartz ampule under vacuum. Prior to use, the substrates were carefully heated in a hydrogen flame to minimize possible surface contaminations as well as possible.

A Pt wire was used as a quasi-reference electrode, and under the applied conditions it has a sufficiently stable electrode potential, which can be well referred to the reversible ferrocene/ferrocinium redox couple. As commonly known, the Pt quasi-reference electrode is not perfect as its electrode potential is easily affected even by slight changes in electrolyte composition. However, if an ultrapure ionic liquid under inert gas conditions is employed, as done in our experiments, the Pt quasi-reference is stable enough, allowing its electrode potential versus a known redox couple such as ferrocene/ferrocinium to be determined. Therefore, we can refer all electrode potentials versus ferrocene/ferrocinium. Only upon a massive electrolysis does the Pt quasi-reference electrode become unstable, in our experience. An advantage, which justifies the use of the Pt quasi-reference, is that a contamination by species from the reference electrode compartment, for example, from Ag/Ag^+, is avoided.

It is still a challenge to construct perfect reference electrodes for STM experiments in ionic liquids. A Pt-ring electrode was used as the counter electrode. There is no dissolution of platinum in this liquid, chlorine evolution or silicon electrodeposition are the counter electrode reactions. For STM experiments mainly in the UPD regime or at the beginning of the bulk deposition Pt is therefore a good counter electrode in this type of ionic liquid. The Pt electrodes were cleaned in a hydrogen flame before use to remove organic impurities.

The electrochemical cell was made of Teflon and clamped over a Teflon-covered Viton O-ring onto the substrate, thus yielding a geometric surface area of the working electrode of 0.3 cm^2. All parts of the electrochemical cell in contact with the electrolyte were formerly cleaned in a mixture of 50:50 vol % H_2SO_4/H_2O_2 followed by refluxing in pyrogene free water (aqua destillata ad iniectabilia) prior to use. The electrochemical measurements were carried out using a PARSTAT 2263 potentiostat/galvanostat controlled by PowerCV software.

The STM experiments were performed with self-built STM heads and scanners under inert gas conditions with a Molecular Imaging PicoScan 2500 STM controller in feedback mode. Assembling of the STM head and filling of the electrochemical cell were performed in a second glovebox solely reserved for assembling of STM heads. The STM head was placed inside an argon-filled stainless steel cylinder, thus ensuring inert gas during STM experiment, transferred to the air-conditioned laboratory with a constant temperature of 23 ± 1 °C, and placed onto a vibration-damped table from IDE. To reduce thermal drift and hysteresis of the piezo to a minimum, the retracted STM scanner was kept scanning overnight with maximum scan range, thus reducing thermal drift as well as possible. STM tips were prepared by electrochemical etching of 0.25 mm 90:10 Pt/Ir wires in 4 M NaCN solution followed by electrophoretical coating with an electropaint from BASF (ZQ 84-3225 0201). During the STM experiments the potential of the working electrode was controlled by the PicoStat from Molecular Imaging. In all experiments the STM pictures were obtained by scanning from the bottom to the top of a picture with a scan rate 2 Hz and a resolution of 512 pixels per line. For the current−voltage tunneling spectroscopy the tip was positioned on the site of interest, and the tip voltage was varied between an upper and a lower limit. During this measurement the feedback is automatically switched off by the software.

To get further information on the deposit, SEM and EDX analyses of electrochemically made thin silicon layers were performed. For this purpose, the working electrode with the deposit on it was removed from the glovebox, washed with 2-propanol to remove the ionic liquid, dried under vacuum, and stored in the glovebox before analysis. For SEM and EDX measurements a high-resolution field emission scanning electron microscope (Carl Zeiss DSM 982 Gemini) was used.

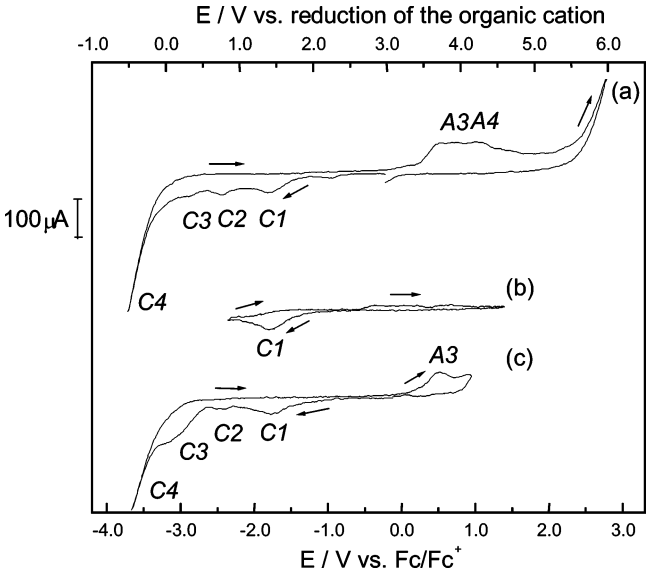

Figure 1. CVs of [BMP]Tf_2N ionic liquid on Au(111) at a scan rate of 10 mV/s and with different reversal potentials. The electrochemical window is ~5 V (a). In the cathodic limit the series of peaks (C1−C3) prior to the massive reduction of the organic cation (C4) are observed. A small reduction peak C3 and its pronounced oxidation counterpart A3 can be ascribed to the adsorption of the organic cation (b, c). The broad oxidation peak (A4) appears only when the cathodic reversal potential is more negative than −2800 mV and is thus correlated with the adsorption (C3) and massive reduction (C4) of the organic cation.

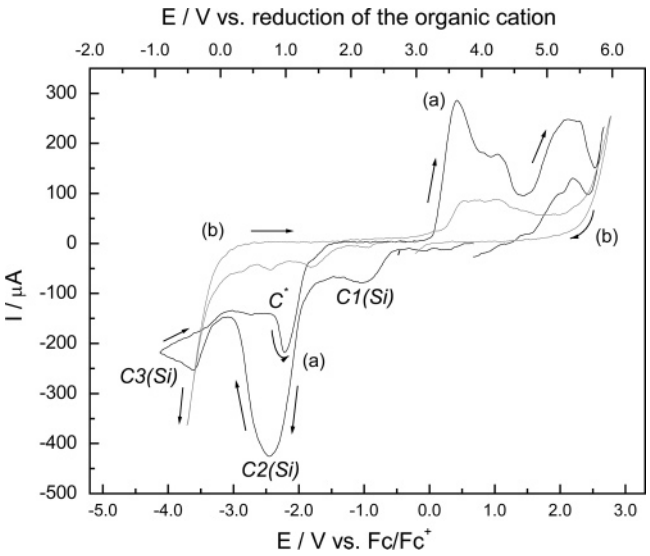

Figure 2. CVs of pure [BMP]Tf_2N ionic liquid (b) and its solution with $SiCl_4$ (0.1 M) (a) on Au(111). The scan rate is 10 mV/s. With the addition of $SiCl_4$ a strong reduction peak C2(Si) correlated with the bulk silicon deposition is observed. The first reduction process C1(Si) is not correlated with a definite surface process. The reduction of the organic cation is hindered on the silicon surface [C3(Si)]. Further silicon deposition is observed also in the reverse scan (C*). Strong oxidation processes at the potential more positive than 0 mV are correlated with the oxidation of cation reduction products, silicon and gold.

Results and Discussion

Cyclic Voltammetry. Cyclic voltammograms of pure [BMP]-Tf_2N ionic liquid on Au(111) acquired at a scan rate of 10 mV/s and with different reversal potentials are presented in Figure 1. The liquid itself, in its dry state, has an electrochemical window of about 5 V on Au(111) (Figure 1a). At the cathodic limit, a series of peaks (C1−C3) preceding the mostly irreversible reduction of the organic cation (C4) has been observed. With the help of the in situ STM we observe a restructuring/reconstruction of the gold surface in the potential regime of peaks C1 and C2 (the respective in situ STM pictures will be presented in the next section). It cannot yet be decided finally if the peaks C1 and C2 are directly correlated with the restructuring/reconstruction. At the anodic limit, we could also observe two oxidation processes, A3 and A4, preceding the bulk oxidation of gold, which starts at +2100 mV versus ferrocene/ferrocinium. All potentials in this work are reported versus ferrocene/ferrocinium if not otherwise stated. The cathodic decomposition limit of this liquid on Au(111), determined from the intersection of the rising decomposition current extrapolated to zero scan rate with the current axis, $I = 0$, is -3200 ± 100 mV versus ferrocene/ferrocinium (see also ref 32). Although it is not a reference electrode potential, we also give the electrode potential as further information versus this decomposition limit in the viewgraphs. To get more information about the electrochemical processes, cyclic voltammetry with varying switching potentials was performed (Figure 1b,c). If the scan is reversed at −2500 mV (Figure 1b), the broad oxidation process from 0 to +1000 mV is not observed, which means this peak must be correlated with the oxidation of the reduction product of the

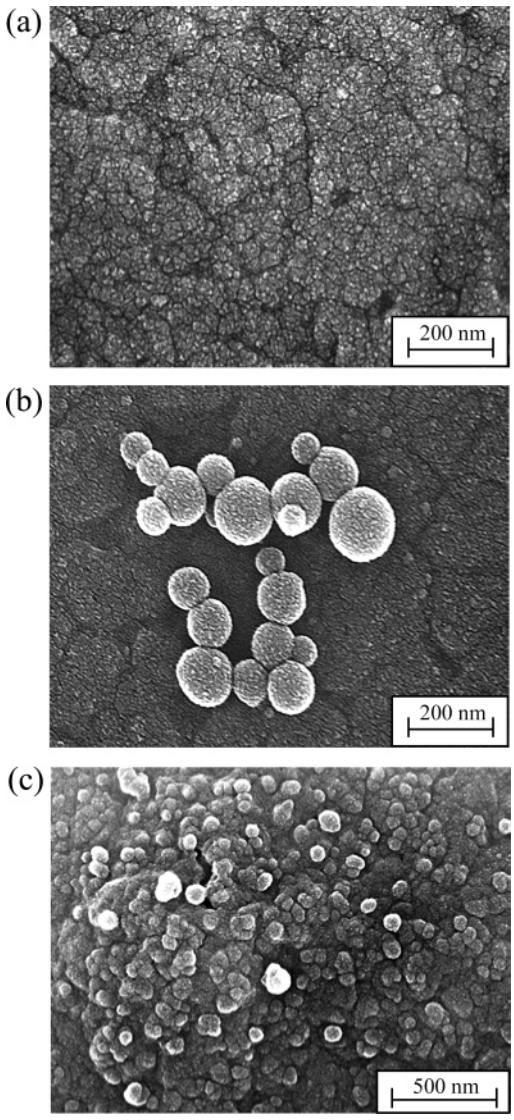

Figure 3. SEM images of gold surface with silicon electrodeposited potentiostatically at −2700 mV versus ferrocene/ferrocinium: (a) SEM image of a 50 nm thick silicon layer composed of individual silicon nanoclusters; (b) a family of globular crystallites of 50−150 nm in diameter built of many small crystals; (c) a 500 nm thick silicon layer consisting of coherent spherical crystallites.

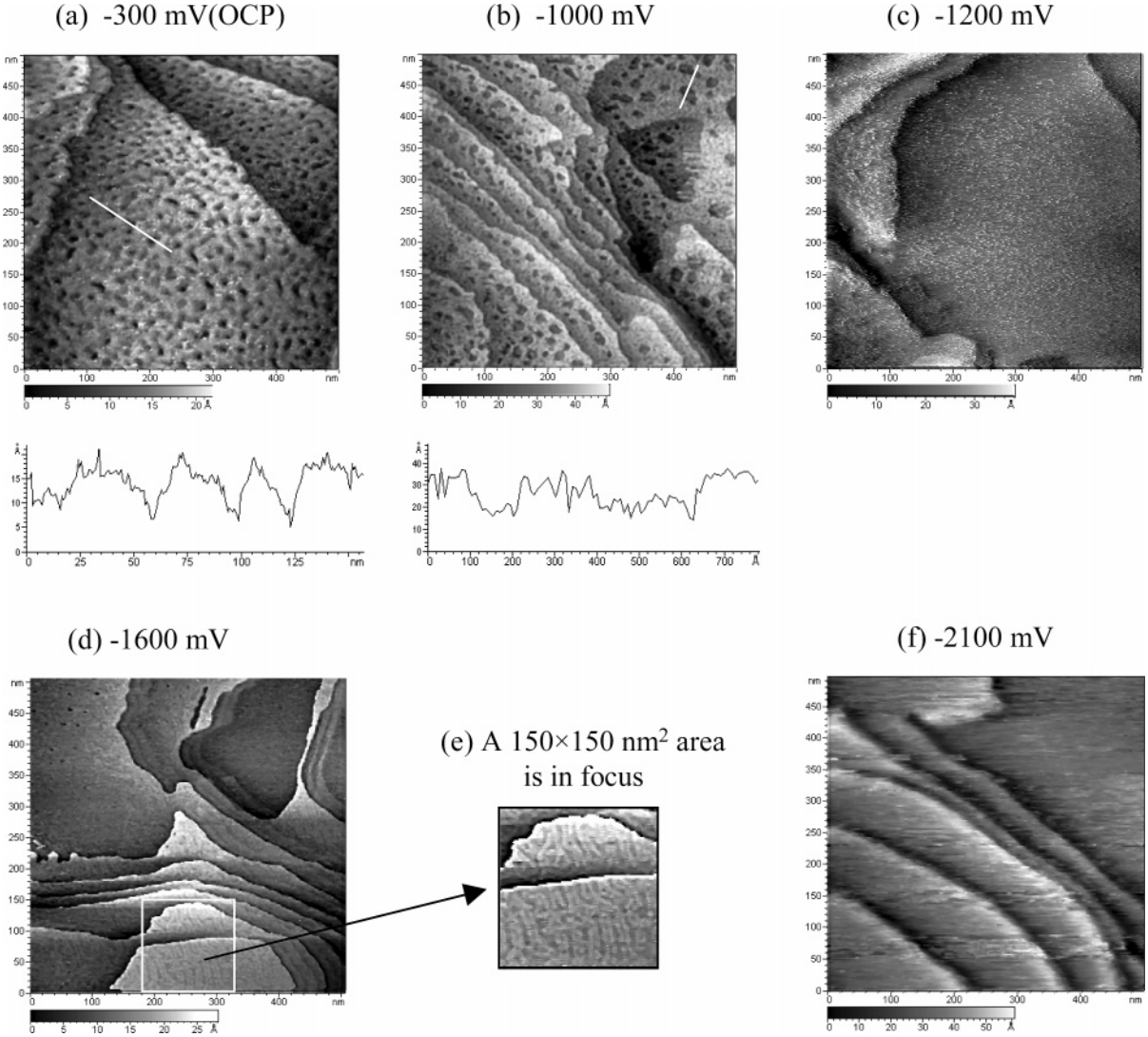

Figure 4. Sequence of STM pictures in the pure [BMP]Tf_2N ionic liquid on Au(111) shows changes of the gold surface by varying the electrode potential. At OCP, −300 mV, a restructured rough gold surface with wormlike structures is observed. The height profile underneath indicates that these nice defects in the surface are monatomic (a). When the electrode potential is decreased to −1000 mV, the surface becomes smoother and the number of holes decreases (b). When the electrode potential is set to more negative values, the holes disappear and some noise appears due to the mobility of the Au atoms at the surface because of its reconstruction (c). At −1600 mV a beautiful reconstructed gold surface is presented. The step height is 250 pm, which is typical of the Au(111) surface (d). When a 150 × 150 mn^2 area is zoomed in on, a long-range superstructure is observed (e). The reconstructed structure is preserved until the adsorption of the organic cation begins (f).

organic cation at C4. The reduction processes C1 and C2 are also present if the cathodic switching potential is at −2800 mV. However, we did not observe defined oxidation processes, which can be correlated without any doubt to C1 and C2. Shortly before the massive reduction of the organic cation begins (C4), a small reduction peak (C3) can be observed, which has an oxidation counterpart A3 (Figure 1c). As we will discuss later, C3 is presumably correlated with adsorption of the organic cation to the Au(111) surface.

Figure 2 compares the electrochemical behavior of pure ionic liquid and of ionic liquid with 0.1 mol/L $SiCl_4$ on Au(111). Upon addition of $SiCl_4$ three reduction processes [C1(Si), C2-(Si), and C3(Si)] are observed in the cathodic regime followed by several oxidation processes in the anodic regime. Process C2(Si) is present only when $SiCl_4$ is in the solution. The cathodic process C3(Si) is due to the reduction of the organic cation on silicon surface. As we have already shown in ref 32, C2(Si) is correlated with the bulk deposition of silicon. It is interesting that the reduction of the cation on the silicon surface is strongly hindered. Process C1(Si) was not observed on HOPG (see ref 32). As there is no deposition in this potential regime (see below) it might be correlated with Au(111) surface restructuring/reconstruction, which is different from the behavior in the pure ionic liquid. We note that the general electrochemical behavior in the cathodic branch on Au(111) in the $SiCl_4$-containing liquid is well reproducible, whereas in the anodic branch the behavior can vary a bit from experiment to experiment. Process C* in the back scan (meaning that a further Si deposition can start in the anodic branch of the CV) is not always observed, revealing that the decomposition of the organic cation might passivate the Si surface. Furthermore, the magnitude and the ratio of the oxidation processes at $E > 0$ mV can vary a bit from experiment to experiment. We could not acquire good STM pictures at $E > 0$ mV. In our opinion these oxidation processes are partly due to Si oxidation (maybe also to silicon surface defects), Au oxidation, and oxidation of cation reduction products. Currently it is an open question as to how $SiCl_4$ dissolves in the liquid and which species is electroactive. Any complexation with the Tf_2N anion or the appearance of Si(II) species as intermediates will have to be investigated in the future. Similar to the work

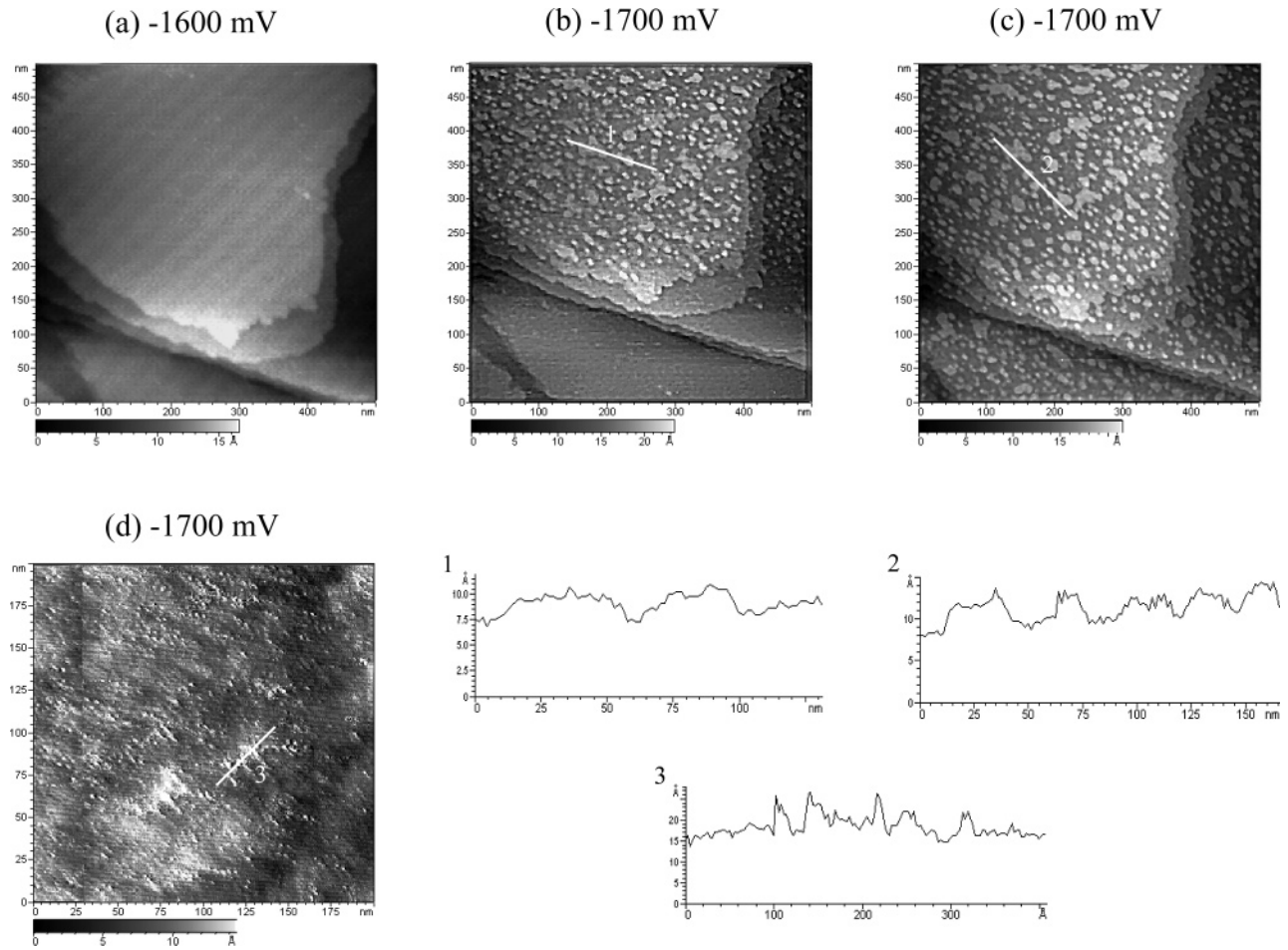

Figure 5. Series of STM pictures showing the growth of silicon in the [BMP]Tf_2N/$SiCl_4$ (0.1 M) on Au(111). At −1600 mV a typical Au(111) structure with a step height of 250 pm is observed (a). If the electrode potential is reduced to −1700 mV, small silicon islands with a width of <60 nm and 150−450 pm in height appear (b, height profile 1). The number of clusters increases in time, and they grow a bit in height (c, height profile 2). After 1 h, a thin silicon layer with some small islands has arisen (d, height profile 3).

done in ref 32, we performed a potentiostatic electrolysis at about −2700 mV for 2 h resulting in a dark deposit on the working electrode surface. Figure 3a shows the gold surface densely covered by a thin silicon layer consisting of clusters of only a few nanometers in width. The thickness of the layer can be estimated roughly to be about 50 nm. In Figure 3b a group of globular crystallites with 50−150 nm in diameter are depicted. It is interesting to mention that these crystals are built of many small clusters cohered in spherical agglomerates. Aggregation of such crystals results in a rough layer of up to 500 nm in thickness (Figure 3c). From the (ex situ) SEM pictures we can conclude that a thin layer of very small clusters/crystallites forms first, followed by crystallite agglomerates that finally lead to a 500−1000 nm thick silicon layer. This is in good agreement with STM results (see below), showing that first small silicon clusters appear on the surface and then a continuous deposit is formed by their merging. The EDX analysis of 500−1000 nm thick layers gave gold, silicon, oxygen, and some chlorine. We can conclude that initially elemental silicon is deposited, which when the electrode is transferred to the air, is subject to some oxidation. We get the same analysis if the deposits are made on pure gold sheets. Unfortunately, the films are too thin to get X-ray diffractograms; therefore, we cannot comment on whether the deposited silicon is crystalline or amorphous.

In Situ STM Results. *Restructuring/Reconstruction of Au(111).* To understand the deposition process better, in situ STM investigations in the pure [BMP]Tf_2N ionic liquid on a Au(111) working electrode were performed. For the STM experiments there was no ferrocene dissolved in the ionic liquid in order to exclude any contamination that could alter the surface processes. All pictures were obtained from bottom to top with a slow scan rate of 2 Hz and a picture resolution of 512 pixels per line. The tip potential was −100 mV versus ferrocene/ferrocinium (calculated) and kept constant during the experiments. The approach was done at the open circuit potential (−300 mV), and then the working electrode potential was slowly changed during scanning toward more negative electrode potentials. As can be seen in Figure 4a, instead of a flat Au(111) surface with terraces, the gold surface is pretty rough with wormlike structures. The Au(111) steps can be recognized, and the average step height is about 250 pm, typical for Au(111). The depth of the defects in the surface seems to be monatomic, as the height profile implies. We can conclude that in [BMP]-Tf_2N at the OCP the Au(111) surface is restructured. When the electrode potential is moved toward more negative values, −1000 mV, the surface becomes smoother (Figure 4b). The steps become better pronounced, and the number of holes in the surface significantly decreases. Furthermore, the depth can be well measured now, and we get values of 150−250 pm, revealing that the defects are only in the topmost gold layer. Upon further decrease of the electrode potential to −1200 mV the holes disappear completely (Figure 4c) and the surface becomes smoother and smoother. However, the surface at −1200 mV appears reproducibly "noisy", and this noise does not disappear before an electrode potential of −1500 mV is

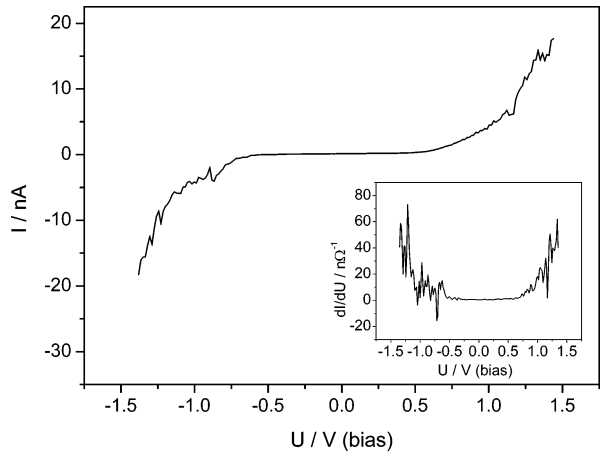

Figure 6. In situ current/voltage tunneling spectrum of a 5 nm thick silicon layer. The spectrum shows clearly the typical semiconducting behavior with a band gap of 1.1 ± 0.2 eV.

reached. In our opinion Au atoms become mobile at the gold surface upon reconstruction, thus leading to some noise in the STM pictures. At −1600 mV (Figure 4d) the gold surface is completely reconstructed and one can see a beautiful Au(111) surface with the typical step height of 250 pm. With increasing resolution (Figure 4e) a long-range superstructure is observed (150×150 nm^2 area is in focus). This gold surface is preserved until about −2100 mV, where the adsorption of the organic cation begins before its massive reduction at −3000 mV starts.

We also investigated how the gold surface changes when the electrode potential is stepped from OCP toward more positive values. The restructured surface is kept until an electrode potential of about +200 mV. At the same time, the number of holes strongly increases and they become smaller and shallower. Upon further increase of the electrode potential, the holes disappear completely. First, the surface becomes smoother, but with time and potential changing to more positive values (+900 mV), the surface roughness increases strongly, making it difficult to acquire good STM pictures. At a potential of about +1300 mV an intensive gold oxidation sets in, which can lead to a complete disintegration of the thin gold film.

Electrodeposition of Silicon. In an earlier paper we presented the first results on the electrodeposition of silicon on highly oriented pyrolytic graphite.[32] HOPG is a difficult substrate for metal or semiconductor deposition as there is only a weak interaction between deposit and substrate. Thus, the STM tip easily pushes away the deposit, making it difficult to get stable and reproducible STM pictures. Nevertheless, we could show that a thin silicon layer of about 100 nm in thickness has a band gap of 1.0 ± 0.2 eV, which is typical of elemental semiconducting silicon. In the present work we aim at getting more information about the process during silicon electrodeposition. We selected Au(111) as an easy to prepare and well-defined substrate. In contrast to "gold on glass", the "gold on mica" substrates from Molecular Imaging deliver wide terraces on almost the whole of the surface and thus deserve—in our opinion—their price. All pictures were taken from bottom to top with a scan rate of 2 Hz and a picture resolution of 512 pixels per line. The working electrode potential was stepped from the OCP toward more negative values. The tip potential was kept constant at −100 mV. Between OCP (−300 mV) and approximately −1600 mV the obtained STM pictures are similar to those taken in the pure ionic liquid; the wormlike surface structure observed at OCP is preserved until a potential of about −600 mV. When the electrode potential is changed to more negative values, noise appears, leading to a decrease in the pictures' quality. We note that compared to the pure ionic liquid in the presence of $SiCl_4$ the quality of the pictures is generally worse until about −1100 mV. In our opinion some halide from $SiCl_4$ makes the surface atoms more mobile, thus leading to a worse quality of the STM pictures. Furthermore, we could not allocate the reduction process C1(Si) to a definite surface process. The smooth gold structure as presented in Figure 4d is already observed at a potential of about −1100 mV and it does not significantly change until −1600 mV. In Figure 5a the surface of Au (111) in [BMP]Tf_2N/$SiCl_4$ (0.1 mol/L) is depicted. We get the typical Au(111) surface with step heights of 250

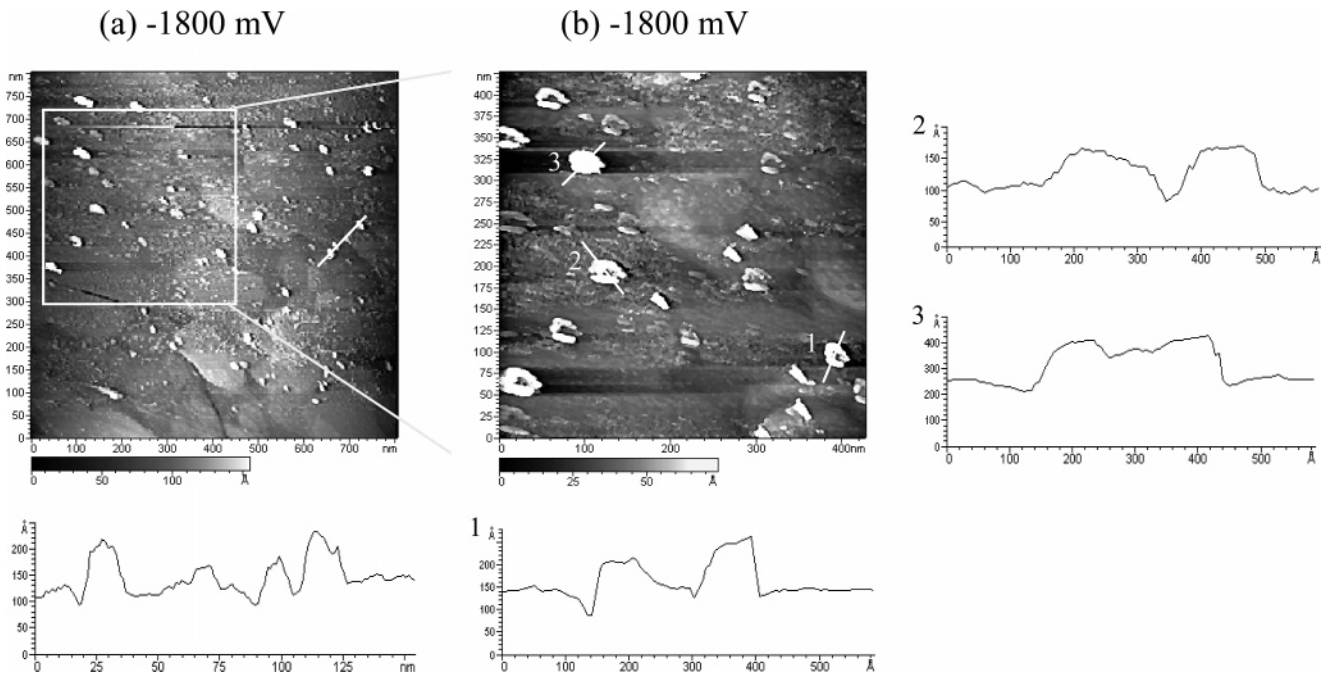

Figure 7. STM images show silicon agglomerate formation on the thin silicon layer (a). A higher resolution shows that the silicon islands grow above the layer and merge laterally, leading to the agglomerates formation, which can be 10 nm in height and 30 nm in width (b, height profiles 1−3).

pm. When the potential is changed from −1600 to −1700 mV, small islands/clusters start to grow (Figure 5b). Height profile 1 shows that the width of these structures is less than 60 nm and their height is between 150 and 450 pm. With time, the number of clusters very slowly increases, and they grow slightly in height (Figure 5c, height profile 2). If we keep the electrode potential constant at −1700 mV for 1 h, the surface is covered completely by a very thin layer of only a few nanometers in height. Furthermore, some small islands rise above this thin layer (Figure 5d). As there is no such deposition process in the pure ionic liquid, this layer is due to the electrodeposition of silicon.

To get more information about the deposit, in situ I/U tunneling spectroscopy was performed on different sites of this only about 5 nm thick layer. Figure 6 shows clearly that there is a potential region of more than 1 V where the tunneling current is zero, revealing that this thin layer has a band gap. Evaluation by dI/dU versus U gives a result that the band gap of this thin layer is 1.1 ± 0.2 eV, the typical value of silicon in the bulk phase.

If the electrode potential is reduced to −1800 mV, the islands begin to grow more rapidly, which leads to the formation of silicon agglomerates (Figure 7a). Silicon islands/clusters grow above the surface of this thin layer and seem to merge laterally. These structures can be as high as 10 nm; their width can reach 30 nm as depicted in Figure 7b and the respective height profiles. A I/U in situ tunneling spectrum of these islands/clusters also gives an average band gap of 1.1 eV. We can conclude that elemental semiconducting silicon has been deposited. Currently, the electrodeposition of Si is investigated in our laboratory in different ionic liquids, as the cation of ionic liquids seems to influence the morphology of the deposits. Furthermore, we aim to investigate the band gap as a function of layer thickness. The results will be reported in a future paper.

Conclusions

In this paper we have presented a detailed in situ STM investigation of Au(111) in the pure ionic liquid 1-butyl-1-methylpyrrolidinium bis(trifluoromethylsulfonyl)imide and of silicon electrodeposition from $SiCl_4$ (0.1 M) in this ionic liquid on Au(111). The pure ionic liquid has an electrochemical window of 5 V on Au(111) limited in the cathodic regime by the irreversible reduction of the organic cation and in the anodic regime by the bulk oxidation of gold. There are three further reduction peaks at about −1700, −2200, and −2800 mV versus ferrocene/ferrocinium. Between OCP (−300 mV) and −1600 mV we observe a restructuring/reconstruction of the gold surface. Between −1600 and −2800 mV the typical Au(111) surface is obtained with a long-range superstructure at −1600 mV. At −2100 mV the STM pictures become noisy, which seems to be correlated with cation adsorption before a massive irreversible reduction begins at potentials below −3000 mV. Upon addition of $SiCl_4$ to the ionic liquid, a similar restructuring/reconstruction is observed, but the pictures are of lower quality. Si deposition on a reconstructed typical Au(111) surface starts on the terraces. Initially small 150−450 pm high islands grow at −1700 mV versus ferrocene/ferrocinium. With time these islands slowly grow, covering the whole of the surface with a few nanometers thick layer after a while. This layer has a band gap of 1.1 ± 0.2 eV, typical for the silicon in the bulk phase. In the cyclic voltammogram the bulk deposition of silicon starts at −1800 mV versus ferrocene/ferrocinium, which is about +1400 mV versus irreversible cation reduction. The irreversible reduction of the organic cation is strongly hindered on the silicon-covered gold, and the respective reduction products seem to passivate the silicon surface. From these experiments we can conclude that elemental semiconducting silicon can be electrodeposited in thin layers. We believe that ultrapure ionic liquids have an enormous potential in studying electrochemical process on the nanoscale with the in situ scanning tunneling microscope. The purity of the liquids is a key factor in STM experiments in ionic liquids, and we can recommend only ultrapure quality for these purposes.

Acknowledgment. An unknown reviewer is gratefully acknowledged for fruitful comments.

References and Notes

(1) Gewirth, A. A., Siegenthaler, H., Eds. *Nanoscale Probes of the Solid/Liquid Interface*; NATO ASI Series E 288; Kluwer Academic Publishers: Dordrecht, The Netherlands, 1995.

(2) Lorenz, W. J., Plieth, W., Eds. *Electrochemical Nanotechnology*; Wiley-VCH: Weinheim, Germany, 1998.

(3) Esplandiu, M. J.; Schneeweiss, M. A.; Kolb, D. M. *Phys. Chem. Chem. Phys.* **1999**, *1*, 4847.

(4) Hagenstrom, H.; Schneeweiss, M. J.; Kolb, D. M. *Langmuir* **1999**, *15*, 7802.

(5) Hagenstrom, H.; Esplandiu, M. J.; Kolb, D. M. *Langmuir* **2001**, *17*, 839.

(6) Kleinert, M.; Waibel, H. F.; Engelmann, G. E.; Martin, H.; Kolb, D. M. *Electrochim. Acta* **2001**, *46*, 3129.

(7) Moller, F. A.; Magnussen, O. M.; Behm, R. J. *Z. Phys. Chem.* **1999**, *208*, 57.

(8) Lachenwitzer, A.; Morin, S.; Magnussen, O. M.; Behm, R. J. *Phys. Chem. Chem. Phys.* **2001**, *3*, 3351.

(9) Polewska, W.; Behm, R. J.; Magnussen, O. M. *Electrochim. Acta* **2003**, *48*, 2915.

(10) Lay, M. D.; Varazo, K.; Stickney, J. L. *Langmuir* **2003**, *19*, 8416.

(11) Lay, M. D.; Varazo, K.; Srisook, N.; Stickney, J. L. *J. Electroanal. Chem.* **2003**, *554*−*555*, 221.

(12) Endres, F. *ChemPhysChem.* **2002**, *3*, 144.

(13) Zein El Abedin, S.; Endres, F. In *Ionic Liquids as Green Solvents*; Rogers, R. D., Seddon, K. R., Eds.; American Chemical Society: Washington, DC, 2003; p 453.

(14) Endres, F. *Z. Phys. Chem.* **2004**, *218*, 255.

(15) Colletti, L. P.; Flowers, B. H.; Stickney, J. L. *J. Electrochem. Soc.* **1998**, *145*, 1442.

(16) Sorenson, T. A.; Lister, T. E.; Huang, B. M.; Stickney, J. L. *J. Electrochem. Soc.* **1999**, *146*, 1019.

(17) Mathe, M. K.; Cox, S. M.; Venkatasamy, V.; Happek, U.; Stickney, J. L. *J. Electrochem. Soc.* **1999**, *152*, C751.

(18) Trindade, T.; O'Brien, P.; Pickett, N. L. *Chem. Mater.* **2001**, *13*, 3843.

(19) Jaiswal, S. L.; Simpson, J. T.; Withrow, S. P.; White, C. W.; Norris, P. M. *Appl. Phys.* **2003**, *A77*, 57.

(20) Bley, R. A.; Kauzlarich, S. M. In *Nanoparticles and Nanocstructured Films: Preparation, Characterization and Applications*; Fendler, J. H., Ed.; Wiley-VCH GmbH: Weinheim, Germany, 1998; p 101.

(21) Agrawal, A. K.; Austin, A. E. *J. Electrochem. Soc.* **1981**, *128*, 2292.

(22) Gobet, J.; Tannenberger, H. *J. Electrochem. Soc.* **1986**, *133*, C322.

(23) Gobet, J.; Tannenberger, H. *J. Electrochem. Soc.* **1988**, *135*, 109.

(24) Fink, C. G.; Dokras, V. M. *J. Electrochem. Soc.* **1949**, *95*, 80.

(25) Szekely, G. *J. Electrochem. Soc.* **1951**, *98*, 318.

(26) Matsuda, T.; Nakamura, S.; Ide, K.; Nyudo, K.; Yae, S. J.; Nakato, Y. *Chem. Lett.* **1996**, *7*, 569.

(27) Katayama, Y.; Yokomizo, M.; Miura, T.; Kishi, T. *Electrochemistry* **2001**, *69*, 834.

(28) Nicholson, J. P. *J. Electrochem. Soc.* **2005**, *152*, C795.

(29) Endres, F. *Phys. Chem. Chem. Phys.* **2001**, *3*, 3165.

(30) Endres, F.; Zein El Abedin, S. *Phys. Chem. Chem. Phys.* **2002**, *4*, 1640.

(31) Endres, F.; Zein El Abedin, S. *Phys. Chem. Chem. Phys.* **2002**, *4*, 1649.

(32) Zein El Abedin, S.; Borissenko, N.; Endres, F. *Electrochem. Commun.* **2004**, *6*, 510.

(33) Kolb, D. M. *Prog. Surf. Sci.* **1996**, *51*, 109.

(34) Lin, L. G.; Wang, Y.; Yan, J. W.; Yuan, Y. Z.; Xiang, J.; Mao, B. W. *Electrochem. Commun.* **2003**, *5*, 995.

(35) MacFarlane, D. R.; Meakin, P.; Sun, J.; Amini, N.; Forsyth, M. *J. Phys. Chem. B* **1999**, *103*, 4164.